Applied Catalysis B: Environmental 220 (2018) 471–476

Contents lists available at ScienceDirect

Applied Catalysis B: Environmental

journal homepage: www.elsevier.com/locate/apcatb

What is the predominant electron transfer process for Au NRs/TiO_2 nanodumbbell heterostructure under sunlight irradiation?

Yuelei Si[a,b], Shuang Cao[a], Zhijiao Wu[a], Yinglu Ji[a], Yang Mi[a], Xiaochun Wu[a,*], Xinfeng Liu[a,*], Lingyu Piao[a,*]

[a] CAS Key Laboratory of Standardization and Measurement for Nanotechnology, CAS Center for Excellence in Nanoscience National Center for Nanoscience and Technology, Beijing, 100190, PR China
[b] University of Chinese Academy of Sciences, Beijing, 100149, PR China

ARTICLE INFO

Article history:
Received 7 June 2017
Received in revised form 29 July 2017
Accepted 3 August 2017
Available online 7 August 2017

Keywords:
Photocatalytic H_2-production
Au nanorods/TiO_2 dumbbell-like heterostructure
Directional charge separation
Electron transfer direction

ABSTRACT

Au nanorods/TiO_2 nano-dumbbells photocatalysts exhibited significantly enhanced visible light photocatalytic H_2-production activity due to injection of hot electrons of photo-excited Au nanorods to TiO_2 nanopaticles, which was confirmed by femtosecond transient absorption spectroscopy. However, it is well known that the electrons were transferred from TiO_2 nanopaticles to Au nanorods under UV light irradiation. Considering the practical application, we investigated the photo-catalytic activity of Au nanorods/TiO_2 nano-dumbbells photocatalysts under sunlight irradiation. Based on the data analysis, we confirmed the dominant electron transfer direction was from TiO_2 nanoparticles to Au nanorods under sunlight irradiation and Au nanorods/TiO_2 nano-dumbbells photocatalysts could act as an effective photocatalyst for H_2-generation from water even without electron donor due to the efficient charge separation and the spatial separation of reduction and oxidation reaction sites.

1. Introduction

Efficient solar-to-fuel conversion is considered as one of the most promising approaches to satisfy the growing demand for clean energy [1–3]. Among the various solar energy harvesting technologies, developing efficient photocatalysts to drive the chemical transformation has received significant attention [4,5]. Hybrid photocatalysts usually demonstrate synergistic features and exhibit more than one function simultaneously [6,7]. In recent years, combination of semiconductor and metal nanoparticles to construct hybrid photocatalysts were intensively investigated and great progresses have been made to optimize the morphology and further improve performance [8–10]. In general, the photocatalytic efficiency is limited by the fast recombination of the photogenerated charge carriers. In order to obtain long-lived charge separation, one-dimensional (1D) nanoheterostructures have emerged as one of the ideal materials due to their quantum confinement in radial dimensions. Especially, the spatial separation structures, such as nanodumbbell heterostructures, offer the opportunity to obtain directed charge separation rather than a random flow direction of photogenerated electrons and holes [11,12]. Up to now, some donor-absorber-reduction catalyst model nanoheterostructures have been successfully synthesized, such as the Pt-tipped CdSe@CdS dot-in-rods [13], Ru-CdSe@CdS-Pt [14], Co-tipped CdSe@CdS nanorods (NRs) [15], Au-tipped CdSe NRs [16] and so on. The photocatalytic results indicated that the photoinduced charge carriers are trapped by the noble metal, which promotes interfacial charge-transfer processes. Therefore, significant efficiency enhancements have been realized by constructing such spatial separation structure. Apart from the metal-tipped semiconductor structures, some nanodumbbell heterostructures based on only metals were also developed, such as Pd-tipped Au NRs [17], Ag_2O-capped Au NRs [18] and so on. However, the semiconductor tipped 1D metal NRs nanoheterostructures were seldom investigated [19].

In our work, we obtained the Au NRs/TiO_2 nano-dumbbells(Au NRs/TiO_2 NDs) composite with the TiO_2 nanoparticles (NPs) only anchored at two ends of Au NRs and made great progress for photocatalytic H_2-production under sunlight irradiation. We investigated how the photocatalytic performances are controlled by the irradiation light. For this Au NRs/TiO_2 NDs composite, hot electrons excited from Au NRs can be injected via a Schottky junction into the conduction band (CB) of TiO_2 NPs for reduction reactions under visible light irradiation, leaving holes in the Au NRs where

* Corresponding authors.
E-mail addresses: wuxc@nanoctr.cn (X. Wu), liuxf@nanoctr.cn (X. Liu), piaoly@nanoctr.cn (L. Piao).

http://dx.doi.org/10.1016/j.apcatb.2017.08.024
0926-3373/

oxidation reaction occurs. However, under UV light irradiation, the photogenerated carriers move in opposite direction. Considering the practical application, it is vital to confirm the predominant electrons transfer process under sunlight irradiation. The present work analyzed the effect of light on the electrons transfer direction from an experimental viewpoint. We believe that this work can provide key information on the carriers transport direction and get more insights into the working principle of these systems under sunlight irradiation.

2. Experimental section

2.1. Experimental materials

All chemical reagents were analytical grade and used without further purification.

Hexadecyltrimethylammoniumbromide (C_{16}TAB) was purchased from Amresco. Methanol (CH_3OH), chlorauric acid ($HAuCl_4{\cdot}3H_2O$), silver nitrate ($AgNO_3$) and titanium (III) chloride solution ($TiCl_3$) were obtained from Beijing Sinopharm Chemical Reagent Co., Ltd. Sodium borohydride ($NaBH_4$), L-ascorbic acid (AA) were obtained from Alfa Aesar. Sodium bicarbonate ($NaHCO_3$) was purchased from Beijing Chemical Works.

2.2. Preparation of gold-seeds

Au NRs were synthesized by a seed-mediated method. C_{16}TAB-capped Au seeds were synthesized by chemical reduction of $HAuCl_4$ with $NaBH_4$: 7.5 mL of C_{16}TAB (0.1 M) aqueous solution was mixed with 100 μL of $HAuCl_4$ (24 mM) and diluted with deionized water to 9.4 mL. Then, 0.6 mL of ice-cold $NaBH_4$ (0.01 M) was added with magnetic stirring. After 3 min, the stirring was stopped and the seed solution was kept undisturbed at 30 °C prior to any further experimentation. The seeds can be used within 2–5 h after preparation.

2.3. Preparation of Au NRs-720 nm

The growth solution of the Au NRs was prepared, which consisted of C_{16}TAB (0.1 M, 100 mL), $HAuCl_4$ (25.5 mL, 1.96 mL), $AgNO_3$ (0.01 M, 1.1 mL) and AA (0.1 M, 0.55 mL). Then 120 μL of seed solution was added to the above growth solution to initiate the growth of the Au NRs. After 12 h, 55 μL of 0.1 M AA was added twice every 30 min. The Au NRs with LSPR at 720 nm were obtained. Then, every 30 mL of Au NRs solution was separated by centrifuging at 9200 rpm for 7 min and dispersed into 5 mL of deionized water (H_2O) as the stock solution.

2.4. Preparation of Au/TiO_2 nano-dumbbells

200 μL of Au NRs stock solution was diluted with 3.8 mL of H_2O and separated by centrifuging at 12000 rpm for 10 min. 3.8 mL of supernatant was extracted and the sedimentary Au NRs were redispersed into H_2O to 1 mL for the following use. 100 μL of 15%–20% $TiCl_3$ was diluted with 2 mL of H_2O. After 490 μL of $NaHCO_3$ solution (1 M) was added into the $TiCl_3$ solution dropwise under stirring, the Au NRs solution was immediately injected. The mixture solution was then stirred for 60 min at room temperature. The prepared Au/TiO_2 nano-dumbbells were washed with ethanol twice and redispersed in ethanol before further use.

2.5. Preparation of Au NRs@TiO_2 core-shell nanostructures

200 μL of Au NRs stock solution was diluted with 1.8 mL of H_2O and separated by centrifuging at 12000 rpm for 10 min. 1.95 mL of supernatant was extracted and the sedimentary Au NRs were redispersed into H_2O to 1 mL for the following use. 100 μL of 15%–20% $TiCl_3$ was diluted with 4 mL of H_2O. After 500 μL of $NaHCO_3$ solution (1 M) was added into the $TiCl_3$ solution dropwise under stirring, the Au NRs solution was immediately injected. The mixture solution was then stirred for 30 min at room temperature. The prepared Au NRs@TiO_2 core-shell nanostructures were washed with ethanol twice and re-dispersed in ethanol before further use.

2.6. Characterization

UV–vis spectra were measured with a Hitachi U-3900 spectrophotometer. Scanning electron microscopy (SEM) images were taken by using the Zeiss electron microscope. Transmission electron microscopy (TEM) images were obtained by using a Tecnai G2 20 S-TWIN electron microscope at an acceleration voltage of 200 kV. High-resolution high-angle annular dark-field scanning transmission electron microscope (HAADF-STEM) and energy dispersive X-ray spectroscopy (EDS) were obtained by using a Tecnai G2 F20 U-TWIN electron microscope. The X-ray diffraction (XRD) patterns of the samples were performed with a SmartLab Goniometer with Cu K-beta radiation, operating at 40 kV and 200 mA. X-ray photoelectron spectroscopy (XPS) analysis was performed on the Thermo Scientific ESCALAB 250Xi spectrometer (all the peaks corrected with reference to the C signal (284.5 eV)). Inductively coupled plasma mass spectrometry (ICP-MS) was used to quantify the amount of Au NRs. The femtosecond transient absorption spectroscopy were tested by time-correlated single-photon counting technique(TCSPC 150). The excitation pusles (wavelength 400 nm) are doubled frequencies of a Mira 900(120 fs, 800 nm, 76 MHz). All the measurements were performed at room temperature and atmospheric pressure with a solid state sample. The EPR spectrum was detected by a Bruker ESP-300E spectrometer at 9.8 GHz, X-band, with 100 Hz field modulation. Samples were illuminated in the cavity of the EPR spectrometer with a 300 W Xe lamp for 10 min.

2.7. Photoelectrochemical measurements

The prepared Au/TiO_2 NDs in ethanol were condensed by centrifugation and coated on an ITO substrate (as-prepared samples as the working electrodes with an active area of ca. 1 cm^{-2}). The electrode was dried in air at 60 °C for 2 h. A standard 3-electrode electrochemical cell was assembled using Ag/AgCl electrode and Pt wire as reference and counter electrodes, respectively. 0.5 M Na_2SO_4 aqueous solution was used as an electrolyte, and the cell was irradiated using a Xe lamp (300 W, Aulight). Linear sweeps and I-t scans were measured at zero bias voltage by a CS310 (CorrTest) electrochemical workstation.

2.8. Photocatalytic H_2 production activity measurements

The prepared Au/TiO_2 NDs dispersed in ethanol were washed with deionized water twice and re-dispersed in water. In a typical photocatalytic H_2-production test, 4 mL of photocatalyst stock solution containing 47.36 μg Au and 64.08 μg TiO_2, which measured by ICP-MS, was diluted with 1 mL of water or 1 mL of methanol to 5 mL in a quartz tube and sealed with a rubber septum. After purging with nitrogen flow for 30 min to remove dissolved air, the suspensions were irradiated for 10 h using a 300 W Xe lamp (Au-light Co.Ltd, Beijing) under magnetic stirring at room temperature or irradiated for 7 h outside (Beijing; 3th, March, 9:30–16:30, 2017). The evolved H_2 in the gas phase was examined by a Techcomp gas chromatography (GC-7900) with a thermal conductivity detector (TCD), 5 Å molecular sieve columns and N_2 carrier.

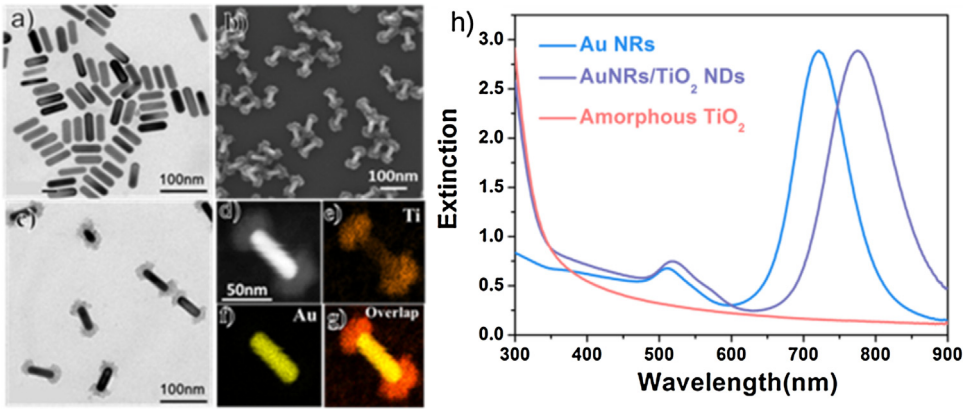

Fig. 1. a) TEM images of bare Au NRs. b) SEM images and c) TEM images of Au/TiO_2 NDs photocatalysts. d–g) HAADF-STEM image and STEM-EDS elemental maps of Au/TiO_2 NDs photocatalysts. h) UV–vis extinction spectra of bare Au NRs (blue line), Au/TiO_2 NDs (purple line) and amorphous TiO_2 (red line) photocatalysts in water. (For interpretation of the references to colour in this figure legend, the reader is referred to the web version of this article.)

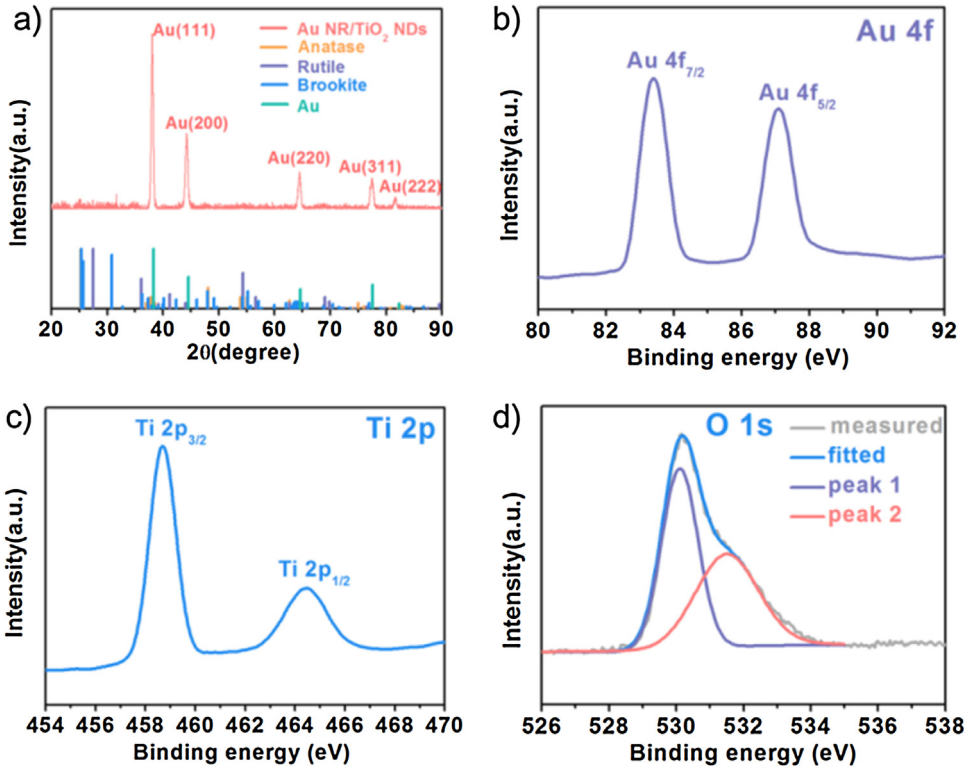

Fig. 2. a) XRD patterns of Au/TiO_2 NDs photocatalysts. XPS of b) Au 4f c) Ti 2p d) O 1s of Au/TiO_2 NDs photocatalysts.

3. Result and discussion

The schematic diagram of the synthesis process is shown in Fig. S1. As shown in Fig. 1a, the bare Au NRs are 21 ± 3 nm in diameter and 62 ± 5 nm in length with an aspect ratio of 3.0 ± 0.3 from TEM image statistic. SEM and TEM images demonstrated that the Au NRs kept the original morphology after loading TiO_2 NPs (Fig. 1b and c). The TiO_2 NPs were selectively anchored on the tips of Au NRs. The thicknesses of TiO_2 clusters were increased with the adding of $NaHCO_3$. When the amount of $NaHCO_3$ is enough, the nanostructures can be change from Au/TiO_2 NDs to Au NRs@TiO_2 NPs core-shell structures (Fig. S2), which confirmed the growth of TiO_2 NPs was started from the tips to the sides of Au NRs. Furthermore, the distribution of each element can be distinctly seen from the HAADF-STEM image and STEM-EDS elemental maps (Fig. 1d–g). The results also confirmed the TiO_2 NPs were mainly distributed on the tips of Au NRs with the sides exposed.

The UV–vis extinction spectrum of bare Au NRs (Fig. 1h, blue line) displayed two SPR bands at 512 and 721 nm, corresponding to their transverse and longitudinal modes, respectively. Because of the loading TiO_2 NPs on the ends of Au NRs, the longitudinal SPR band of the Au/TiO_2 NDs photocatalysts (Fig. 1h, purple line) displayed an obvious red shift with a peak at 775 nm, which was due to the increase of the refractive index of the surrounding environment [20]. At the same time, the absorbance of the Au/TiO_2 NDs photocatalyst at UV region (<350 nm) has been enhanced. No obvious shift in the absorption edge is observed for Au/TiO_2 NDs compared with amorphous TiO_2 NPs at UV region, indicating that the existence of Au NRs does not alter the property of TiO_2 NPs. By contrast, the transverse SPR band changed slightly (a red shift < 10 nm). Furthermore, with the various amount of TiO_2 NPs, the light absorption

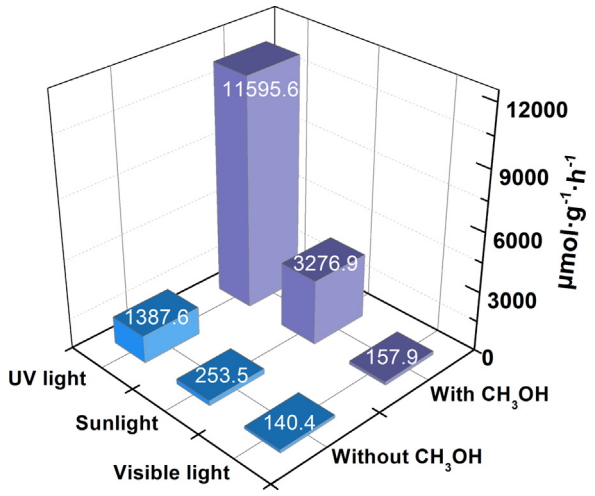

Fig. 3. Comparison of photocatalytic H_2-evolution activities of Au/TiO_2 NDs under visible, UV light irradiation or natural sunlight (Beijing, Mar. 3th, 9:30-16:30, 2017) irradiation in methanol aqueous solution (purple) or pure water (blue). (For interpretation of the references to colour in this figure legend, the reader is referred to the web version of this article.)

range can be tailored and covered across a broad spectrum from visible to near-infrared region (Fig. S3).

The XRD results (Fig. 2a) showed five appreciable sharp diffraction peaks, which were assigned to the highly crystallographic Au NRs. No apparent diffraction peaks belonging to TiO_2 NPs were observed. Herein, the deposited TiO_2 NPs derived from hydrolysis of $TiCl_3$ were amorphous. Because of the H_2 bubbles produced during the reaction, the TiO_2 shells presented the porous morphology [21]. In order to elucidate the valence states of individual elements of the materials, X-ray photoelectron spectroscopy (XPS) was performed. The full survey spectra of the Au/TiO_2 NDs photocatalysts confirmed the presence of Au, Ti, and O (Fig. S4). The Au 4f binding energies are present double peaks and located at 83.4 eV and 87.1 eV, respectively, with the splitting of 3.7 eV, which indicates the metallic nature of Au (Fig. 2b) [20]. High-resolution XPS spectra of Ti 2p exhibits two strong peaks located at 458.65 eV (Ti $2p_{3/2}$) and 464.5 eV (Ti $2p_{1/2}$), respectively, and confirms the Ti^{4+} state (Fig. 2c) [23]. The XPS peak of O 1 s is asymmetric and fitted into two peaks, corresponding to Ti—O (530.1 eV) and O—H (531.5 eV), respectively. The weaker O—H peak is attributed to the surface species, such as Ti—OH, resulting from the chemisorbed water on the TiO_2 surface (Fig. 2d) [24].

Confirming the transfer direction of the photogenerated carriers is the key point to optimize the efficiency of the hybrid nanoheterostructure. In this work, we firstly investigated the effect of light on the H_2-generation rates and concluded the electron transfer rules for the prepared Au/TiO_2 NDs. As shown in Figs. 3 and S5, either under visible or UV light irradiation, a certain amount of hydrogen can be detected in the pure water or methanol aqueous solution. The mechanism of CH_3OH as holes (h^+) scavenger for hydrogen production from water was shown in Fig. S6. After 10 h of UV light irradiation, 12.9 μmol H_2 was produced and the related efficiency was 11595.6 μmol g^{-1} h^{-1} with respect to the Au-TiO_2 mass by the assist of methanol, which is even higher than that of the reported one dimentional Pt-tipped CdS hybrid (5000 μmol g^{-1} h^{-1}, λ = 360–440 nm) [11]. By contrast, the value was 157.9 μmol g^{-1} h^{-1} under visible light irradiation under the same conditions. It is speculated that two possible factors that lead to the wide difference of photocatalytic efficiency under UV and visible light irradiation. Firstly, great differences of electron transfer direction and transfer efficiency exist under different light irradiation. Under UV light irradiation, the photogenerated electrons mainly come from TiO_2 NPs and transfer to Au NRs, which act as the hydrogen production active sites [25,26]. Under visible light irradiation, by exciting surface plasmons in the Au NRs, a Schottky junction on the plasmonic metal/semiconductor interface can select out the hot electrons and the tip-loaded TiO_2 NPs accept the photogenerated hot electrons coming from Au NRs [27,28]. Simultaneously, the electrons coming from Au could transfer back, which can be confirmed by the femtosecond transient absorption (TA) spectroscopy that discussed subsequently. Therefore the efficiency of photogenerated eletron separation and transfer is much lower under visible light irradiation compared with UV light irradiation. Apart from that, the difference of photogenerated electron density is another significant factor that result in such phenomenon. In order to ascertain the assumption, transient photocurrent measurements were conducted (Fig. S7). The photocurrent densities under UV light irradiation are much higher than that of under visible light irradiation, indicating that an enhanced charge transportation from TiO_2 NPs to Au NRs under UV light irradiation. Based on the results, it is obvious that more photogenerated electrons can be formed under UV light irradiation for the Au/TiO_2 NDs hybrid.

In view of the practical application, natural sunlight is the light source, herein, it is essential to confirm the predominant electron transfer process under full-wave band irradiation. It can be depicted that the H_2-evolution rate achieved 3276.9 μmol g^{-1} h^{-1} in the presence of methanol under sunlight irradiation, which is much higher than that of visible light irradiation (Fig. 3). Considering the H_2-generation efficiency under UV-light irradiation was also much higher than that of visible light irradiation and the photocurrent density results, we can conclude that the electron transfer from TiO_2 NPs to Au NRs plays a dominant role under sunlight irradiation. In order to evaluate the H_2-production efficiency under sunlight irradiation, Pt-TiO_2 hybrid was synthesized and investigated as a contrast. As shown in Fig. S8, the Pt nanoparticles were loaded by the wide accepted in situ photo-deposited method with the Pt weight percentage of 0.1 wt%. The photocatalytic results showed that 975.7 μmol H_2 was obtained after 7 h of sunlight irradiation (Fig. S9). It means that the H_2 production efficiency of the Pt-TiO_2 hybrid is 13938 μmol/(g·h). Although the present Au NRs/TiO_2 nanodumbbell hybrid could not be comparable to Pt-TiO_2, this work can provide key information on the carriers transport direction and get more insights into the working principle of these nanodumbbell heterostructures with spatial separation under sunlight irradiation.

In order to confirm the electron transfer direction under visible light, femtosecond transient absorption (TA) spectroscopy was used to investigate exciton and carrier dynamics under visible light irradiation. After 400 nm excitation, bare TiO_2 NPs demonstrate a neglectable signal due to the fact that TiO_2 NPs process none absorption at this region (Fig. 4a). Whereas the Au NRs show a strong absorption feature between 450 and 525 nm at early delay time and decays fast, herein, a bleach of exciton band are formed. By contrast, only a bleach signal was detected near 700 nm (Fig. 4b). The results illustrated that the electrons in the long axis direction process a faster transfer rate. For the Au/TiO_2 NDs, a long-lived exciton state can be clearly observed at wavelength between 570 and 650 nm and a bleach signal also formed subsequently (Fig. 4c). Therefore, we can speculate that the existence of the tip-coated TiO_2 can efficiently promote the charge separation of the Au NRs. The long-lived exciton state in the long axis direction of Au NRs can also be confirmed by the TA kintetics results. As depicted in Fig. 4d and e, when excited at 400 nm, a neglectable difference can be detected at 532 nm between Au NRs, TiO_2 NPs and Au/TiO_2 NDs, whereas, when probed at 711 nm, the Au/TiO_2 NDs show a significant long-lived excition state. Based on the above results and analyses, we can conclude that a charge separation state formed in the long axis direction of Au NRs for the Au/TiO_2 NDs under visible light irradiation. Herein, the electrons were transferred from Au

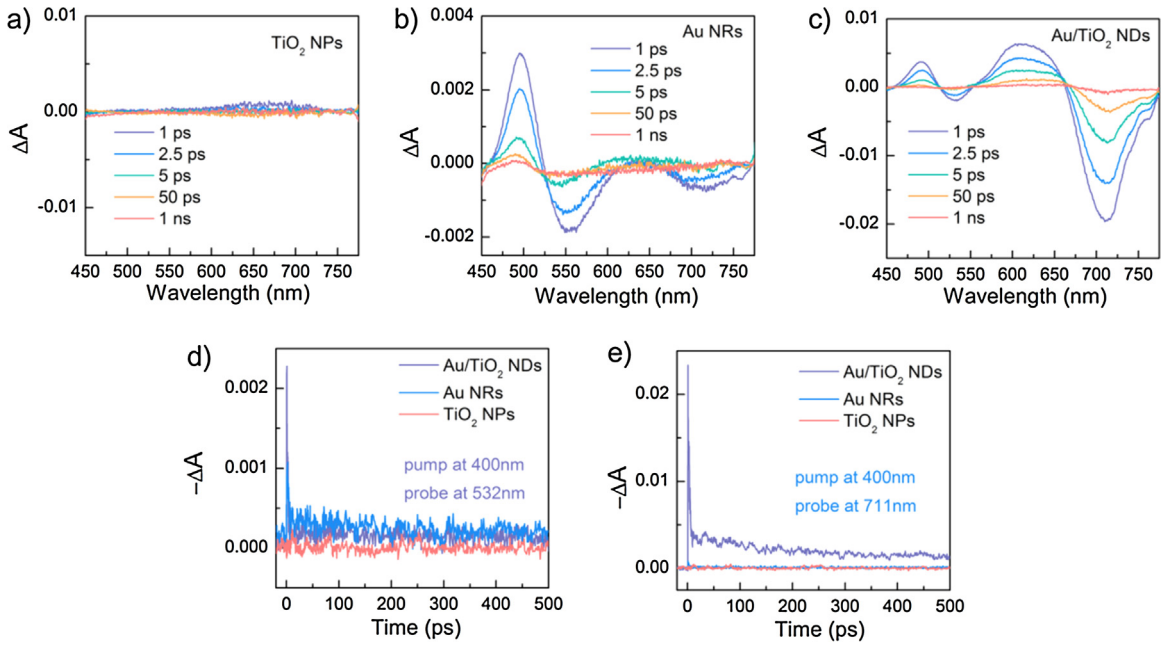

Fig. 4. TA spectra of (a) TiO_2 NPs, (b) Au NRs and Au/TiO_2 NDs, respectively, at indicated delay time windows after 400 nm excitation. TA kintetics for Au/TiO_2 NDs after 400 nm excitation and detected at (d) 532 nm and (e) 711 nm, respectively.

NRs to TiO_2 NPs under visible light irradiation. At the same time, the much longer lived excition state in the long axis direction of Au NRs also indicates that the generated electrons could shock between Au NRs and TiO_2 NPs. Due to the relative low loading weight of TiO_2 NPs, no evident signal can be detected when excitated by UV light. But, combining the photocatalytic results, we can draw a conclusion that the photogenerated electrons transferring from TiO_2 NPs to Au NRs played the leading role under UV or sunlight irradiation rather than the LSPR effect of Au NRs.

Much to our delight, the Au/TiO_2 NDs nanostructures also demonstrated a relative high H_2-production rate in the absence of sacrificial agent, which confirmed the well-designed photocatalyst can successfully achieve efficient spatial charge separation no matter under UV or visible light irradiation. The spatial separation of reduction and oxidation reaction sites was achieved subsequently. The H_2-evolution rate can reach up to 1387.6 $\mu mol\ g^{-1}\ h^{-1}$ under UV light irrdiation without sacrificial agent. However, no oxygen was detected and it is speculated that the holes are captured by ^{-}OH and lead to the formation of $^{\bullet}OH$ (Fig. S10). Furthermore, it should be noticed that a H_2-evolution rate of 140.4 and 253.5 $\mu mol\ g^{-1}\ h^{-1}$ was achieved under visible light and sunlight irradiation from pure water, respectively. In order to confirm the advantages of the dumbbell-like nanostructures, we also obtained the Au NRs@TiO_2 NPs core-shell nanostructures as a reference (Fig. S11). No hydrogen can be detected in the absence of electron donor no matter under sunlight, UV and visible light irradiation (Fig. S12). In addition, with the assistance of sacrificial agent, the Au NRs@TiO_2 NPs nanostructures also showed a much lower H_2-production efficiency under the same experimental conditions, which further comfirmed the superiority of the Au/TiO_2 NDs nanostructures. Combining the photocatalytic and photocurrent results, we can speculate that the difference of photogengerated electron density is the pivotal factor resulting in the diverse of photocatalytic efficiency under different light irradiation. Due to the low electron density under visible light irradiation, there is limited hot electrons can transfer from Au NRs to TiO_2 NPs. Therefore, the consumption rate of holes has a little effect on the H_2-production efficiency, which lead to the similar catalytic rate whether the existence of electron donor or not. Whereas, with the assistance of CH_3OH, the H_2-production efficiency is 13 times higher than that of without methanol under sunlight irradiation. The results indicated that when the electron density at a high level, the hole consumption rate play a significant role in enhancing the photocatalytic activity.

Although very few similar dumbbell shaped structures have been reported up to now, there is no doubting that the well-designed hybrid can facilitate efficient long-lasting charge carrier separation and minimize back reaction of intermediates. Control experiments indicated that the pure Au NRs and amorphous TiO_2 NPs exhibited no activity for H_2-production. Herein, the results confirmed that this Au/TiO_2 NDs hybrid with spatial charge separation can be acted as an efficient H_2-production photocatalyst under natural sunlight irradiation.

Based on the above analysis, the mechanism of the enhanced photocatalytic water splitting efficiency is proposed as follows: When a visible light irradiation source was used, Au NRs acted as light harvester due to their LSPR effect [29,30]. The hot electrons excited from Au NRs could be injected via a Schottky junction into the conduction band of tip-coated TiO_2 NPs. Then, the sides of Au NRs were covered by positive charges. Simultaneously, the electrons were involved in the generation of H_2, while the leaving holes could be consumed by CH_3OH. At the same time, part of electrons could transfer back from TiO_2 to Au NRs. Under UV light irradiation, TiO_2 NPs was excited to generate electrons (e^-) and holes (h^+), the electrons in conduction band of TiO_2 NPs were injected to Au NRs due to the lower Fermi level of Au NRs [31]. As a result, the individual positively charged TiO_2 NPs region and negatively charged Au NRs region were formed. Subsequently, the H_2 were produced on the surface of Au NRs. Under natural sunlight irradiation, the directed spatial partition of charge carrier also formed in Au/TiO_2 NDs photocatalyst, however, the Au NRs acted as a H_2-production reaction site.

4. Conclusions

In conclusion, we synthesized the Au nanorods/TiO_2 nanodumbbell photocatalyst with directed spatial partition of charge carrier. The spatial separation of reduction and oxidation reaction sites was achieved subsequently. Especially, the characteristics of

the spatial charge separation could be altered with the change of the irradiation light. In order to cater to the practical application, we discussed the dominant electron transfer direction under natural sunlight irradiation is form TiO_2 NPs to Au NRs. The photocatalytic results also indicated that due to the efficient spatial charge separation, the hybrid could act as an effective photocatalyst in pure water without electron donor under solar light irradiation. The difference of photogengerated electron density is the pivotal factor resulting in the diverse of photocatalytic efficiency under different light irradiation. The present results demonstrated a novel and effective strategy to achieve effective water splitting. The profound studies to optimize the morphology and improve the charge separation efficiency are on the way.

Acknowledgements

We acknowledge the financial support by the Ministry of Science and Technology of China (Nos. 2016YFA0200902 and 2016YFF0203803), and the 'Strategic Priority Research Program' of the Chinese Academy of Sciences (Grant No XDA09040200). The author would like to thank the team members of >Xiaoying Qi, Huaiqiu Chang and Chi Zhang for their help in finishing this work. Yuelei Si and Shuang Cao contributed equally to this work.

Appendix A. Supplementary data

Supplementary data associated with this article can be found, in the online version, at http://dx.doi.org/10.1016/j.apcatb.2017.08.024.

References

[1] T.R. Cook, D.K. Dogutan, S.Y. Reece, Y. Surendranath, T.S. Teets, D.G. Nocera, Chem. Rev. 110 (2010) 6474–6502.
[2] X. Li, J.G. Yu, M. Jaroniec, Chem. Soc. Rev. 45 (2016) 2603–2636.
[3] D.J. Lampert, H. Cai, A. Elgowainy, Energy Environ. Sci. 9 (2016) 787–802.
[4] X. Li, J.G. Yu, S. Wageh, A.A. Al-Ghamdi, J. Xie, Small 12 (2016) 6640–6696.
[5] H.X. Han, C. Li, Natl. Sci. Rev. 2 (2015) 145–147.
[6] H. Kisch, Angew. Chem. Int. Ed. 25 (2013) 812–848.
[7] K.F. Wu, T.Q. Lian, Chem. Soc. Rev. 45 (2016) 3781–3810.
[8] J.H. Yang, D. Wang, H.X. Han, C. Li, Acc. Chem. Res. 46 (2013) 1900–1909.
[9] Y. Xu, R. Xu, Appl. Surf. Sci. 351 (2015) 779–793.
[10] X.Q. Li, J. Locozzia, Y. Wang, X. Cui, Y.H. Chen, S.Q. Zhao, Z. Li, Z.Q. Lin, Energy Environ. Sci. 10 (2017) 402–434.
[11] M. Berr, A. Vaneski, A.S. Susha, J. Rodríguez-Fernández, M. Döblinger, F. Jäckel, A.L. Rogach, J. Feldmann, Appl. Phys. Lett. 97 (2010) 093108.
[12] K.P. Acharya, R.S. Khnayzer, T. O'Connor, G. Diederich, M. Kirsanova, A. Klinkova, D. Roth, E. Kinder, M. Imboden, M. Zamkov, Nano Lett. 11 (2011) 2919–2926.
[13] P. Kalisman, Y. Nakibli, L. Amirav, Nano Lett. 16 (2016) 1776–1781.
[14] L. Amirav, F. Oba, S. Aloni, A.P. Alivisatos, Angew. Chem. Int. Ed. 54 (2015) 7007–7011.
[15] L.J. Hill, N.E. Richey, Y. Sung, P.T. Dirlam, J.J. Griebel, E. Lavoie-Higgins, I.B. Shim, N. Pinna, M.G. Willinger, W. Vogel, J.J. Benkoski, K. Char, J. Pyun, ACS Nano 8 (2014) 3272–3284.
[16] E. Shaviv, O. Schubert, M. Alves-Santos, G. Goldoni, R.D. Felice, F. Vallée, N.D. Fatti, U. Banin, C. Sönnichsen, ACS Nano 5 (2011) 4712–4719.
[17] Z.K. Zheng, T. Tachikawa, T. Majima, J. Am. Chem. Soc. 137 (2015) 948–957.
[18] Z.H. Bo, Z.H. Sun, M.D. Xiao, H.J. Chen, L.W. Tian, J.F. Wang, J. Mater. Chem. 21 (2011) 11537–11543.
[19] B.H. Wu, D.Y. Liu, S. Mubeen, T.T. Chuong, M. Moskovits, G.D. Stucky, J. Am. Chem. Soc. 138 (2016) 1114–1117.
[20] C.H. Fang, H.L. Jia, S. Chang, Q.F. Ruan, P. Wang, T. Chen, J.F. Wang, Energy Environ. Sci. 7 (2014) 3431–3438.
[21] R. Liu, A. Sen, J. Am. Chem. Soc. 134 (2012) 17505–17512.
[23] M.G. Wang, J. Han, H.X. Xiong, R. Guo, Y.D. Yin, ACS Appl. Mater. Interfaces 7 (2015) 6909–6918.
[24] X. Zhang, Y. Liu, S.T. Lee, S.H. Yang, Z.H. Kang, Energy Environ. Sci. 7 (2014) 1409–1419.
[25] C.G. Silva, R. Juárez, T. Marino, R. Molinari, H. García, J. Am. Chem. Soc. 133 (2011) 595–602.
[26] J.J. Chen, J.C.S. Wu, P.C. Wu, D.P. Tsai, J. Phys. Chem. C 115 (2011) 210–216.
[27] D. Kumar, A. Lee, T. Lee, M. Lim, D.K. Lim, Nano Lett. 16 (2016) 1760–1767.
[28] A. Furube, L. Du, K. Hara, R. Katoh, M. Tachiya, J. Am. Chem. Soc. 129 (2007) 14852–14853.
[29] Z.W. Seh, S. Liu, M. Low, S.Y. Zhang, Z. Liu, A. Mlayah, M.Y. Han, Adv. Mater. 24 (2012) 2310–2314.
[30] A. Primo, A. Corma, H. García, Phys. Chem. Chem. Phys. 13 (2011) 886–910.
[31] M. Murdoch, G.I.N. Waterhouse, M.A. Nadeem, J.B. Metson, M.A. Keane, R.F. Howe, J. Liorca, H. Idriss, Nat. Chem. 3 (2011) 489–492.

Further reading

[22] M.J. Wang, J. Han, H.X. Xiong, R. Guo, Langmuir 31 2015 6220-6228.